Boosted activity by engineering the enzyme microenvironment in cascade reaction: A molecular understanding

Jing Wang [a,1], Haiyang Zhang [b,1], Deping Yin [a,1], Xiao Xu [c], Tianwei Tan [a], Yongqin Lv [a,*]

[a] Beijing Key Laboratory of Bioprocess, College of Life Science and Technology, Beijing University of Chemical Technology, Beijing, 100029, China
[b] Department of Biological Science and Engineering, School of Chemistry and Biological Engineering, University of Science and Technology Beijing, Beijing, 100083, China
[c] School of Chemical Engineering, Nanjing University of Science and Technology, Nanjing, 210094, China

ARTICLE INFO

ABSTRACT

Engineering of enzyme microenvironment can surprisingly boost the apparent activity. However, the underlying regulation mechanism is not well-studied at a molecular level so far. Here, we present a modulation of two model enzymes of cytochrome *c* (Cty C) and D-amino acid oxidase (DAAO) with opposite pH-activity profiles using ionic polymers. The operational pH of poly (acrylic acid) modified Cyt C and polyallylamine modified DAAO was extended to 3–7 and 2–10 where the enzyme activity was larger than that at their optimum pH of 4.5 and 8.5 by 106% and 28%, respectively. The cascade reaction catalyzed by two modified enzymes reveals a 1.37-fold enhancement in catalytic efficiency compared with their native counterparts. The enzyme activity boosting is understood by performing the UV–vis/CD spectroscopy and molecular dynamics simulations in the atomistic level. The increased activity is ascribed to the favorable microenvironment in support of preserving enzyme native structures nearby cofactor under external perturbations.

1. Introduction

Enzymes possessing superior chemo-, regio-, and stereo-selectivity have been extensively applied in the production of pharmaceutical drugs, fine chemicals, biofuels, etc [1–7]. However, the industrialization of free enzymes in solution is often impeded by their ease of denaturation or deactivation. The directed protein evolution or site-directed mutagenesis is one of the powerful approaches to create tailor-made enzymes that meet the application demands [8–14]. Another simple and effective strategy is immobilization or chemical modification of enzymes that facilitates increased stability and enables the recovery and reuse of enzyme catalysts [15–26]. But a reduced activity is often observed during the immobilization or chemical modification processes owing to the unfavorable conformational transition or blockage of the active sites [17,27].

In recent years, notable studies have demonstrated that some well-designed chemically modified or immobilized enzymes may exhibit higher apparent activities than their native counterparts [28–36]. In particular, there have been great interests focusing on the engineering of enzyme microenvironment [36–41], which emphasizes the modulation

of local chemical environment of enzymes to achieve the optimal conditions close to natural ones despite of the unfriendly conditions in the bulk environment. For example, in an interesting study, Zhang et al. described the microenvironment engineering of cytochrome C (active at acidic conditions) using a negatively charged polyelectrolyte, which enabled a 10-times throughput increase in cascade reaction together with a second enzyme D-amino acid oxidase (active at basic conditions) [42]. Other studies also demonstrate that the conjugation of enzymes with ionic polymers or DNA nanostructures extends the pH-activity profiles of enzymes by altering the protein surface charge or aggregation state, and thus enhancing the enzyme activity at different pHs [35, 42–49]. However, the modulation mechanism is complicated and not well-studied at a molecular level so far.

On the other hand, in practical applications, multienzyme systems containing two or more enzymes are usually involved to attain the synergistic biocatalysis [16,50–54]. The maximum catalytic efficiency can be achieved if the catalytic activity of each enzyme is fully explored. However, each enzyme has their own inherent characteristics, and the operational condition for the multienzyme system typically adopts a compromised parameter that is not the optimal value for any of the

---

individual enzyme [17,51]. The mismatch of the optimum reaction conditions may significantly decrease the catalytic efficiency of the cascade reaction. Engineering of enzyme microenvironment may conquer this limitation so that the individual enzyme can work in tandem with each other to achieve good compatibility.

Here in this work, the mechanism underlying the pH-modulation of microenvironment of two enzymes by attaching ionic polymer chains has been elucidated on the molecular level by molecular dynamics simulation. Inspired by Zhang's work [42], two model enzymes (cytochrome C, Cyt C; D-amino acid oxidase, DAAO) with opposite pH-activity profiles were selected. The oxidation of D-alanine by DAAO/O_2 produces pyruvic acid and H_2O_2 intermediate. Cyt C then catalyzes the oxidation reaction of amplex red with H_2O_2 to resorufin (Scheme 1a). The anionic and cationic polyelectrolytes were employed to engineer the local pH microenvironment of two enzymes for cascade reactions. We observed that the introduction of ionic polymer chains could actually engineer the protonation/deprotonation in the proximity of enzyme active sites, thereby boost enzyme activity. The combination of anionic and cationic polyelectrolytes enhanced the compatibility of multienzymes, and extended the optimum operational pH range of the cascade reaction.

2. Experimental

2.1. Synthesis of Cyt C-PAA and DAAO-PAM conjugates

The grafting of Cyt C with poly (acrylic acid) (PAA) was carried out via the *N*-(3-dimethylaminopropyl)-*N*′-ethylcarbodiimide hydrochloride/*N*-hydroxysulfosuccinimide (EDC/NHS) coupling approach. Before the reaction, a stock solution of 30 μM Cyt C was first prepared by dissolving 2 mg Cyt C in 5.5 mL phosphate buffer (50 mM, pH 8.5). In a typical reaction, 20.6 mg EDC was added to 5.5 mL 900 μM PAA solution. The mixture was stirred for 5 min followed by adding 27.5 mg sulfo-NHS and stirring continuously for another 15 min. Then, 5.5 mL 30 μM Cyt C was mixed with the activated PAA and stirred for 16 h at room temperature. The obtained Cyt C-PAA conjugate was dialyzed for three days using a dialysis bag (M_w = 7,000) to remove the unreacted compounds.

The grafting of DAAO with polyallylamine (PAM) was also performed via the EDC/NHS coupling approach. A stock solution of 3 μM DAAO was first prepared by dissolving 1 mg DAAO in 4.32 mL phosphate buffer (50 mM, pH 6). Then, 16.2 mg EDC was added to 4.32 mL 180 μM PAM solution. The mixture was stirred for 5 min followed by adding 21.6 mg sulfo-NHS and stirring continuously for another 15 min. Then, 4.32 mL 3 μM DAAO was mixed with the activated PAM and stirred for 16 h at room temperature. The obtained DAAO-PAM conjugate was dialyzed for three days using a dialysis bag (M_w = 20,000) to remove the unreacted compounds.

2.2. Enzymatic activity assays

The enzyme activity assays were performed using a Multiskan Spectrum plate reader (Thermo Fisher Scientific, USA) in a clear 96-well plate. H_2O_2 and 2,2′-azino-bis(3-ethylbenzothiazoline-6-sulphonic acid) (ABTS) were utilized as substrates to study the activity of free Cyt C and
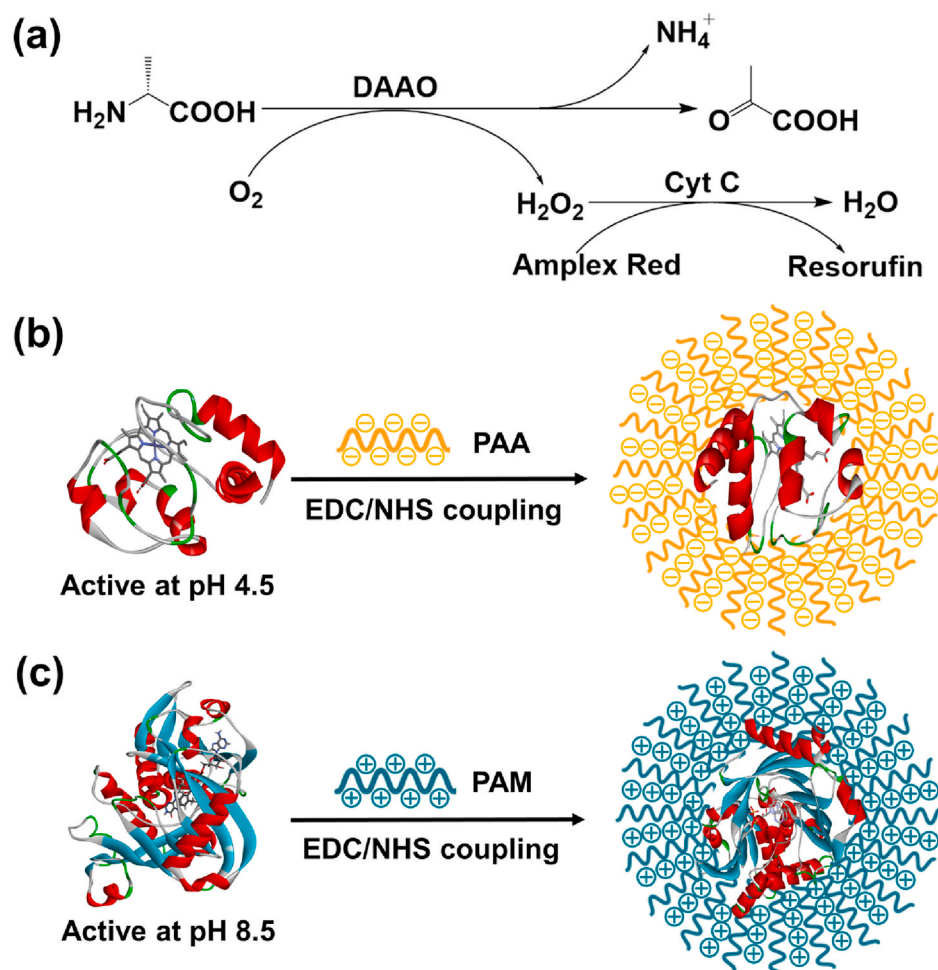
Scheme 1. Schematic illustrations for the DAAO/Cyt C cascade reaction (a), the synthesis of Cyt C-PAA (b) and DAAO-PAM (c) conjugates via the EDC/NHS coupling approach.

Cyt C-PAA conjugate. The final assay solution comprises 1 μM Cyt C, 20 mM H_2O_2, and 5 mM ABTS in 50 mM phosphate buffer at different pH values ranging from 2 to 10. The absorbance increase at 415 nm was recorded for 2 min.

To assess the activity of DAAO in an extended pH range of 2–10, the oxidation of $_D$-alanine catalyzed by DAAO was carried out at different pH values. The assay solution contains 100 nM DAAO and 100 mM $_D$-alanine. After the enzymatic reaction for 5 min, the product solution was adjusted to pH 7. Then 200 nM horseradish peroxidase (HRP) and 100 μM amplex red in 50 mM phosphate buffer were added to the above solution. The absorbance increase at 572 nm was recorded for 2 min.

2.3. Cascade kinetics study

The study of cascade kinetics of DAAO-PAM/Cyt C-PAA compared to native DAAO/Cyt C was carried out using $_D$-alanine and amplex red as substrates. The concentration of $_D$-alanine ranged from 5 mmol/L to 400 mmol/L. After 5 min, the reaction was terminated using concentrated hydrochloric acid followed by adjusting the mixture to neutral. Then, 100 μM amplex red in 50 mM phosphate buffer was added to the mixture. The absorbance increase at 572 nm was recorded for 2 min.

2.4. Thermal stability study

The stock solutions of free enzymes (0.5 mg DAAO and 0.8 mg Cyt C dissolved in 1 mL phosphate buffer saline at pH 7.0) and chemically modified enzymes (0.5 mg DAAO-PAM and 0.8 mg Cyt C-PAA dispersed in 1 mL phosphate buffer saline at pH 7.0) were first prepared. The effects of temperature on the residual enzymatic activity were determined with 20 μL of the stock solution added to 420 μL 50 mmol/L phosphate buffer saline at pH 7. The enzyme solutions were kept at temperatures of 30, 60, and 90 °C for 3 h, followed by adding the substrate solution containing 100 μL 100 mmol/L $_D$-alanine and 30 μL 100 μmol/L amplex red. The residual enzyme activity was calculated by recording the absorbance increase at 572 nm for 2 min.

2.5. Molecular dynamics simulation

The crystal structures of Cyt C (PDB code: 2B4Z) with a resolution of 1.50 Å and DAAO (PDB code: 3W4J) with a resolution of 2.74 Å extracted from the Protein Data Bank were used as initial configurations for molecular dynamics (MD) simulations. The protonation states of Cyt C and DAAO at different pH values (2, 4.5, 7, 8.5, and 10) were determined by a web server H++ [55]. Poly (acrylic acid) (PAA) and poly-allylamine (PAM) with a degree of polymerization of 5 were used to link with Lys residues in Cyt C and Asp/Glu residues in DAAO, respectively. This mimicked a modification of Cyt C with negatively charged polymers and of DAAO with positively charged polymers. The proteins of Cyt C and DAAO were modeled with the Amber ff14SB force field [56]. Force field parameters of the cofactor heme in Cyt C and flavin adenine dinucleotide (FAD) in DAAO were taken from the AMBER parameter database archived by Prof. Richard Bryce (http://research.bmh.manche ster.ac.uk/bryce/amber). The modified residues of PAA-Lys (with a net charge, −4), PAM-Asp (net charge, +4), and PAM-Glu (net charge, +4) were optimized at HF/6-31G* in gas phase using the Gaussian 09 software [57], and restrained electrostatic potential (RESP) charges were calculated with the help of "antechamber" tool [58].

To find out the available Lys or Asp/Glu residues that can be covalently modified by PAA or PAM, the accessible surface area (ASA) or solvent accessibility of amino acids in Cyt C or DAAO was calculated using the online server ASA-View [59]. The spiral diagrams in Fig. S1a and Fig. S2a showed the spatial distribution of amino acid residues in Cyt C and DAAO. The exposed residues were located at the outer ring, and large spherical radius corresponded to high solvent accessibility. Lys residues with a high solvent accessibility are much easier to be modified with ionic polymers. Fig. S1b showed the solvent accessibility of

different Lys residues in Cyt C, and the ones with a solvent accessibility (SA) higher than 0.5 were modified. Based on different degrees of modification, we obtained three conjugates denoted as Cyt C-[PAA]$_n$ (n = 4, 7, 10), where n signified explicitly the number of the short PAA chain being grafted. For example, Cyt C-[PAA]$_4$ represented four Lys residues in Cyt C (SA>0.7, K86, K22, K73, K25) were modified with short PAA chains, and this conjugate had the lowest PAA grafting density. Cyt C-[PAA]$_7$ suggested seven Lys residues in Cyt C (SA>0.6, K86, K22, K73, K25, K8, K88, K5) were modified with short PAA chains. Cyt C-[PAA]$_{10}$ indicated ten Lys residues in Cyt C (SA>0.5, K86, K22, K73, K25, K8, K88, K5, K87, K79, K39) were modified with short PAA chains, and this conjugate had the highest PAA grafting density. Similarly, Figs. S2(b and c) showed the solvent accessibility of different Asp/Glu residues in DAAO, and the ones with a SA value higher than 0.5 were selected. According to different grafting densities, four conjugates were obtained named as DAAO-[PAM]$_n$ (n = 4, 8, 12, 17), where n implied the number of the short PAM chain being grafted. For instance, DAAO-[PAM]$_4$ represented 4 residues (one Asp and three Glu) in DAAO (SA>0.9, D109, E220, E85, E100) were grafted with short PAM chains. DAAO-[PAM]$_8$ indicated 8 residues (two Asp and six Glu) in DAAO (SA>0.7, D109, D58, E220, E85, E100, E154, E165, E249) were grafted with short PAM chains. DAAO-[PAM]$_{12}$ suggested 12 residues (five Asp and seven Glu) in DAAO (SA>0.6, D109, D58, D123, D66, D127, E220, E85, E100, E154, E165, E249, E336) were grafted with short PAM chains. DAAO-[PAM]$_{17}$ signified 17 residues (seven Asp and ten Glu) in DAAO (SA>0.5, D31, D58, D66, D73, D109, D123, D127, E85, E100, E154, E165, E173, E220, E249, E261, E335, E336) were grafted with short PAM chains.

All simulations were carried out using GROMACS 2018 package [60]. The protein-cofactor configuration was solvated in a box of TIP3P water molecules with a minimum distance of 1.0 nm between protein and box edge. Sodium and chlorine ions were then inserted into the box to neutralize the simulated system with a salt concentration of 0.15 mol/L. The simulation system was first optimized by 10,000 steps of energy minimization. The positions of heavy atoms of solutes were then constrained, and the water molecules and salt ions were relaxed during a 100 ps NVT equilibration, followed by a 100 ps NPT equilibration using the Parrinello-Rahman barostat [61,62]. Finally, a 100 ns molecular dynamic simulation was performed under the NPT with a time step of 2 fs. The temperature was maintained at 300 K using a Nose-Hoover thermostat, and the coupling time was set to 0.1 ps. The electrostatic interactions were calculated using the particle mesh Ewald (PME) method [63,64]. The Visual Molecular Dynamics (VMD) software [65] was employed to analyze the simulation configurations. The root-mean-square deviations (RMSD), root-mean-square fluctuation (RMSF), radial distribution function (RDF), solvent-accessible surface area (SASA), and number of hydrogen bonds were calculated with the GROMACS tools.

3. Results and discussion

3.1. Characterizations of Cyt C-PAA and DAAO-PAM conjugates

The multienzyme system containing Cyt C and DAAO was selected for the proof-of-concept. Cyt C has an optimal pH of 4.5, and DAAO is intrinsically active at pH 8.5 [42,66]. The anionic PAA and cationic PAM were respectively employed to engineer the inherent pH dependence of Cyt C and DAAO by surface grafting via the EDC/NHS coupling approach (Scheme 1).

The hydrodynamic diameters of Cyt C-PAA and DAAO-PAM conjugates were 122 and 123 nm, which were larger than the sizes of native Cyt C (4.5 nm) and DAAO (8.6 nm) as determined from dynamic light scattering (DLS) measurements [Figs. S3(a and b) in the supporting information]. The zeta potential of Cyt C decreased from −2.36 to −12.05 mV after conjugating with the negatively charged PAA. And the grafting of positively charged PAM increased the zeta potential of DAAO from

−3.02 to 25.35 mV. The titration curves of Cyt-PAA and DAAO-PAM conjugates in Figs. S3(c and d) displayed a molar ratio of 1:13.6 for Cyt C/PAA and 1:66.5 for DAAO/PAM, confirming the high grafting density of ionic polymers on the protein surface.

Cyt C in its native conformation displays a prominent Soret band maximum at ∼ 409 nm (π-π* transition), a position representing low spin state ion, a form arising from the heme's axial ligand, His[18] and Met[80] [67–69]. The Cyt C-PAA conjugate reflected identical UV–vis spectra to its free enzyme in solution [Fig. 1a, b], suggesting that PAA grafting did not alter the ground state properties of Cyt C [68,70]. However, a blue shift of 7–9 nm or a red shift of 3 nm of the Soret band was observed for both free Cyt C and Cyt C-PAA conjugate when conditioning at pH 2 or 10, implying the denaturation of Cyt C with His[18] and/or Met[80] replaced thereby with iron in its high spin state [67,68, 70].

The variations in the secondary structure (far-UV), tertiary structure (near-UV), and heme environment (Soret CD) of Cyt C in the absence and presence of PAA at different pHs were also investigated by circular dichroism (CD) spectroscopy. Far-UV spectroscopy in the range of 200–250 nm reflects the secondary structure alterations of Cyt C

induced by the backbone orientation [67–69]. Fig. 1c showed prominent negative peaks at 208 nm and 222 nm typical of helical proteins. After the introduction of PAA or changing the pH to 2, a reduction of the negative side peak along with a red shift was observed implying the perturbation of secondary structures (Fig. 1f), which resembled the phenomenon obtained from the UV–vis spectra. The identical CD spectra in the near-UV spectrum (265–300 nm) range confirmed the preservation of the tertiary structure of Cyt C [Fig. 1d, g]. The Soret-CD spectra provides information related to the native structure of Cyt C in the proximity of heme. The Soret region in CD spectra features a strong positive band at 406 nm and a strong negative peak at 417 nm. The former corresponds to the heme-globin interactions and the heme-Fe spin state, and the latter represents Met80-Fe and Phe82-heme interactions [67–69]. The Soret region CD in Fig. 1e, h exhibited minor or no change between native Cyt C and Cyt C-PAA conjugate indicating PAA grafting did not alter the heme environment. However, the variation of pH conditions induced a blue shift for the positive peak at 406 nm, suggesting the possible perturbations of heme-globin interactions and heme-Fe spin state. These results suggested that upon PAA grafting, only the secondary structure of native Cyt C was varied. But at
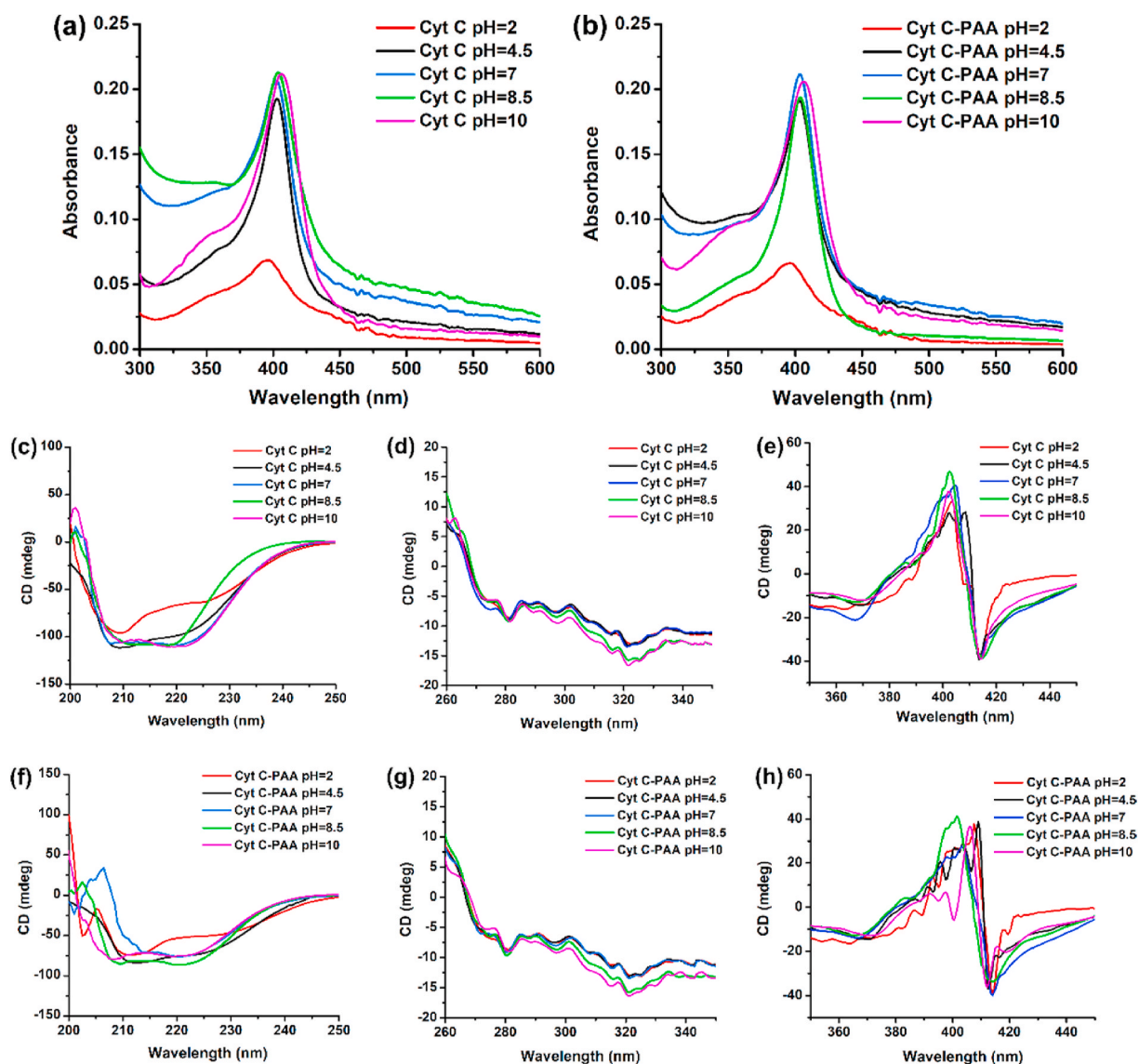
Fig. 1. UV–vis spectra of native Cyt C (a) and Cyt C-PAA conjugate (b) in the range of 300–600 nm at different pH values. Far-UV CD spectra (c and f), near-UV spectra (d and g), and Soret region UV-CD spectra (e and h) of native Cyt C (c–e) and Cyt C-PAA conjugate (f–h) at different pH values. The concentration of native Cyt C and Cyt C-PAA conjugate was 1.3×10^{-7} mol/L.

unfavorable pHs, both the secondary structure and heme environment were disturbed causing the denaturation of Cyt C not only in the native state but also in its conjugate one.

With respect to DAAO, the native DAAO and DAAO-PAM conjugate revealed identical UV–vis and CD spectra (Fig. S4) implying that PAM grafting did not alter the conformational structures of DAAO (secondary structure, tertiary structure, and cofactor FAD environment).

3.2. PAA and PAM polyelectrolytes boost the activity and stability of Cyt C and DAAO

The activity assays were carried out to evaluate the catalytic performances of Cyt C and DAAO in the presence of ionic polymers.

The peroxidase-like activity of Cyt C and Cyt C-PAA conjugate was measured by a colorimetric approach using H_2O_2 and ABTS as substrates. Both native Cyt C and the Cyt C-PAA conjugate exhibited the highest activity at pH 4.5 (Fig. 2a), suggesting that its optimum pH was 4.5 and the protonated PAA did not affect the inherent biological activity of Cyt C. Compared with native Cyt C, the Cyt C-PAA conjugate exhibited boosted activity with 205.6% and 183.3% improvements of its maximum activity at pH 4.5 and 7, and maintained 99.9% of its maximum activity at pH 3. The optimum pH of Cyt C was extended from 4.5 to 3 ∼ 7. Similar finding was also reported by Zhang et al. in which the conjugation of Cyt C with polymethacrylic acid (PMAA) exhibited the pH range of Cyt C to 4.5 ∼ 7 [42]. However, with increasing pH to 10 or decreasing pH to 2, the activity of native Cyt C or Cyt C-PAA conjugate was reduced dramatically due to the perturbation of secondary structures as suggested from the UV–vis and CD spectra in Fig. 1.

The activity of DAAO was determined by catalyzing the oxidation of D-alanine with oxygen accompanied by the generation of hydrogen peroxide (H_2O_2). Horseradish peroxidase (HRP) was then employed to catalyze the reaction between H_2O_2 and neutral *N*-acetyl-3,7-

dihydroxyphenoxazine (amplex red) with a stoichiometry of 1:1 producing resorufin which was a pink-colored fluorescent product [42]. As seen in Fig. 2b, native DAAO and DAAO-PAM conjugate showed the highest activity of 449.2 U/mg at the optimum pH 8.5. The activity of native DAAO was also greatly influenced by the pH conditions. Only 68.1% and 48.5% of its maximum activity were retained at pH 10 and 2. By contrast, the DAAO-PAM conjugate displayed significantly enhanced activity in a wide pH range of 2–10. And 106.1%, 128.2% and 103.7% of its maximum activity were retained at pH 10, 8.5, and 2, suggesting that PAA grafting extended the optimum pH range of DAAO toward more acidic conditions by 6.5 pH units and toward more alkaline conditions by 1.5 pH units. This excellent catalytic performance exceeds the properties reported in previously published studies. For example, the use of highly charged polyanionic insoluble carriers for enzyme immobilization extended the optimal pH of several proteolytic enzymes by 1–3 units [38–40]. The optimum pH of trypsin was shifted from 7.8 to 8.0 when it was covalently linked with carboxyl-terminated poly [3-dimethyl (methacryloyloxyethyl) ammonium propane sulfonate] [41]. The optimal pH of chymotrypsin altered from 10 to 8 when conjugating with a cationic polymer [44]. In our case, PAM provided an alkaline microenvironment in the vicinity of DAAO active sites, which not only stabilized the secondary and tertiary structures but also preserved the FAD crevice as suggested from the UV–vis and CD spectra in Fig. S4, thereby facilitating an enhanced enzyme activity at a wide pH range. It is worthy of note that DAAO is a dimeric enzyme [70]. The monomer-monomer interactions play an important role to maintain the stability of DAAO. The chemical modification of DAAO with PAM could also prevent the dissociation of its dimeric state and increase the enzyme stability.
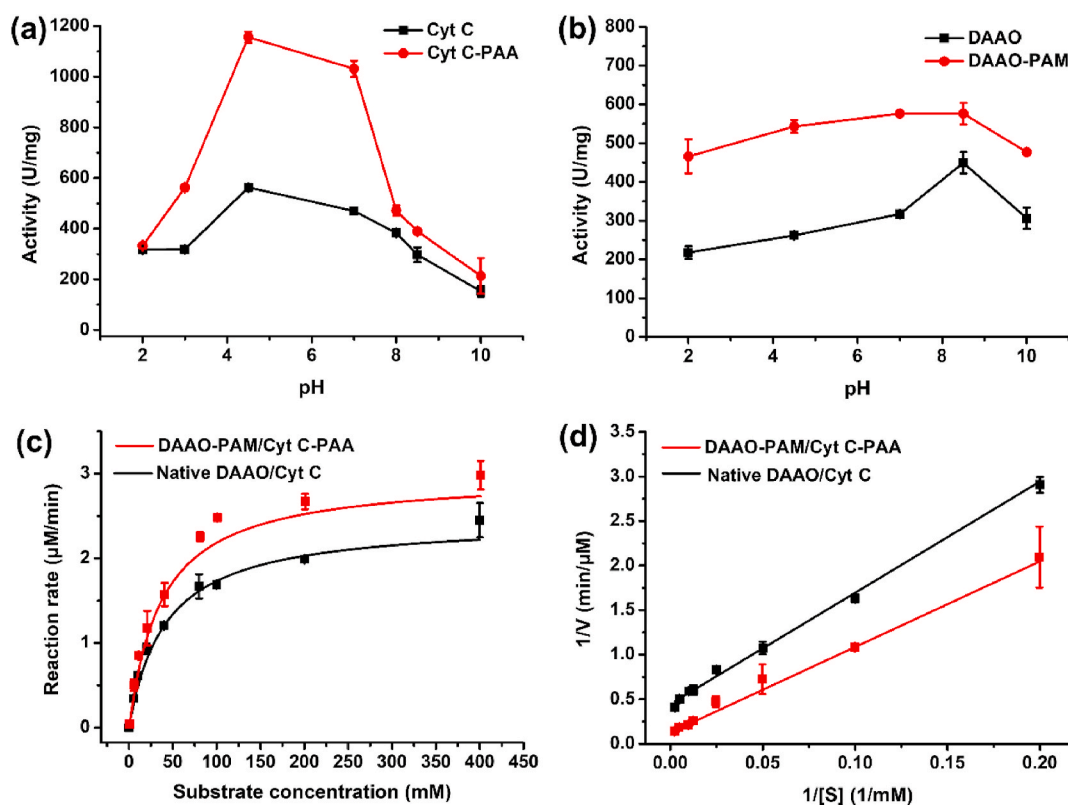
Fig. 2. pH-Activity profiles of native Cyt C and Cyt C-PAA conjugate (a), and native DAAO and DAAO-PAM conjugate (b). Kinetic plots (c) and the corresponding Lineweaver-Burk plots (d) depicting cascade reactions catalyzed by DAAO-PAM/Cyt C-PAA conjugates in comparison to free DAAO/Cyt C in solution. The enzyme activities of free enzyme and enzyme-polymer conjugate were shown as U per mg enzyme.

3.3. Cascade reactions catalyzed by DAAO-PAM/Cyt C-PAA

We then evaluated the enhanced performances in cascade reactions catalyzed by DAAO-PAM/Cyt C-PAA via modulating the enzyme microenvironment using ionic polymers. DAAO can oxidize $_D$-alanine with oxygen into pyruvic acid producing H_2O_2 which functions as substrate of Cyt C. The kinetic parameters k_{cat} and K_M of DAAO-PAM/Cyt C-PAA compared with native DAAO/Cyt C were calculated from the kinetics curves and Lineweaker-Burk linearization plots [Fig. 2c, d]. As shown in Table 1, the apparent K_M was equal implying that the polyelectrolytes modified enzymes had similar affinity toward the substrate compared to native DAAO/Cyt C. The DAAO-PAM/Cyt C-PAA system displayed an increased k_{cat} suggesting the enhanced enzyme activity after grafting, which was in good agreement with the results shown in Fig. 2b. An increased k_{cat}/K_M value of 18.34 mM s^{-1} was obtained, that was 1.37-fold higher than the native enzymes. These results clearly demonstrated that engineering of local pH microenvironment of enzymes using ionic polymers could not only boost enzyme activity of single enzyme but also improve the catalytic efficiency of cascade reactions by promoting the compatibility and synergistic effect of multienzymes.

3.4. A molecular understanding of the activity boosting mechanism studied by MD simulation

The activity boosting mechanism at the molecular level underlying the pH-engineering of enzyme microenvironment by attaching ionic polymers was studied by MD simulations. We first studied the characteristics of Cyt C and DAAO at different pH values using MD simulation. According to the optimum pH of 4.5 for Cyt C and 8.5 for DAAO [42,71], five pHs (2, 4.5, 7, 8.5, and 10) in line with experiments were selected. Root-mean-square deviation (RMSD), radius of gyration (R_g), solvent-accessible surface area (SASA), and secondary structures were analyzed to characterize the grafted enzymes. The RMSD value is an indicator of conformational changes along the trajectory compared to the crystal structure [72]. Low RMSD value suggests that the conformational structure of enzyme is closer to its native state, and thus the enzyme may well maintain its original activity. As presented in Fig. S5 in the supporting information, the RMSD for all the simulation systems leveled off after 100 ns, confirming the equilibration of the system as well as the validity of force field and parameters used.

The Cyt C simulation systems displayed lower RMSD values at pHs of 4.5, 7, and 8.5 suggesting stable conformational structures at these pH values (Fig. S6a). The higher RMSD values at pH 2 or 10 indicated larger conformational changes compared with its crystal structure, which might be one of the reasons for the low enzyme activity of Cyt C at these pH values. The R_g value can be used to describe the compactness of protein structures [73], and SASA reveals the thermodynamic stability of an enzyme [72]. Compared with pH 2 and 10, the lower R_g and SASA at pH 4.5–8.5 suggested the more compact structures [Figs. S6(b and c)]. The secondary structures of Cyt C at different pH values were evaluated as well, and partially destroyed structures were observed at unfavorable pH conditions especially at pH 10 (Fig. S6d), consistent with the far-UV CD spectra in Fig. 1c. Similarly, Fig. S7 showed the simulation results for DAAO at a pH range of 2–10. Evaluation of RMSD, R_g, SASA, and secondary structures confirmed that DAAO had more native and compact structures at pH 7 and 8.5, which could explain the high enzyme activity of DAAO at these pH values.

Table 1
Kinetic parameters of cascade reaction catalyzed by native DAAO/Cyt C and DAAO-PAM/Cyt C-PAA conjugates.

Catalyst	K_m (mM)	k_{cat} (s^{-1})	k_{cat}/K_m (mM s^{-1})
Native DAAO/Cyt C	28.01	0.37	13.3
DAAO-PAM/Cyt C-PAA	28.35	0.52	18.3

3.4.1. Anionic PAA enhances the activity and stability of Cyt C identified by MD simulation

The optimum catalytic pH of Cyt C is 4.5, and thus we chose anionic poly (acrylic acid) (PAA) to create a local acidic microenvironment in the vicinity of Cyt C. Fig. S1c depicted the electrostatic surface potentials of Cyt C and its conjugates with PAA as a function of pH values. As expected, higher grafting density of negatively charged PAA on the protein surface corresponded to lower electrostatic surface potential, which agreed well with the zeta potential result. The electrostatic map of Cyt C revealed the distribution of charged patches on the protein surface (Fig. 3a). The grafting of PAA increased the SASA value of Cyt C (Fig. S8a). The number of hydrogen bonds between Cyt C and water also raised with the increase of PAA grafting density due to the introduction of carboxylic acids (Fig. S8b).

We then investigated the enhancement of Cyt C activity in the presence of PAA. As indicated from the significantly reduced RMSD for Cyt C-[PAA]$_4$ conjugate (Fig. 3b), appropriate PAA grafting facilitated the enhancement of enzyme stability. Notably, excessive PAA grafting might produce steric hindrance and result in reduced enzyme activity. For example, Cyt C-[PAA]$_{10}$ featuring higher PAA grafting density showed larger RMSD values, suggesting its inferior enzyme activity. To further elucidate the deactivation mechanism of Cyt C when conjugating with a plethora of PAA, we studied the radial distribution functions (RDF) between the active catalytic site heme and Lys residues that were modified with PAA. As seen in Fig. 3c, while the Cyt C-[PAA]$_7$ and Cyt C-[PAA]$_4$ conjugates only showed one prominent peak at 1.25–2.25 nm, the Cyt C-[PAA]$_{10}$ conjugate displayed two characterisitic peaks centered at 0.25–0.75 and 1.25–2.25 nm. This demonstrated that the chemical modification of Lys residues in Cyt C-[PAA]$_{10}$ conjugate occurred at the position where the heme-Lys distance was in the range of 0.25–0.75 nm and 1.25–2.25 nm. The first modification position was very close to heme, and as a result the excessive chemical modification might generate steric hindrance and cause the decrease of Cyt C activity. Although the CD spectra in Fig. 1c-h revealed changes in the secondary structures of Cyt C before and after grafting with PAA, no significant variation was observed from the simulation result (Fig. S9).

The twenty key amino acids that interacted noncovalently with heme in the crystal structure of Cyt C were analyzed (Fig. S10). The root-mean-square fluctuation (RMSF) of the twenty key amino acid residues was calculated to evaluate their local dynamic variations. The residues that undergo high structural changes and fluctuations during the simulation were accordingly identified. The RMSF of native Cyt C was intensified at its non-optimal pHs, indicating the structural changes and conceivable enzyme denaturation mentioned above (Fig. S11a). After the appropriate modification with PAA, the fluctuations of residue side chains in Cyt C-[PAA]$_4$ conjugate were diminished at a pH range of 4.5–8.5, implying its increased pH tolerance [Fig. S11(c-e)]. It is worthy of note that, the RMSF of Cyt C-[PAA]$_4$ was strengthened at pH 2 or 10 compared to native Cyt C in spite of the smaller RMSD values [[Figs. S11 (b and f)], suggesting a big fluctuation of the residue side chains regardless of the small structural changes of backbone orientation. This phenomenon was in coincidence with the UV–vis and CD spectra in Fig. 1, and could explain the result in Fig. 2a why the activity of Cyt C-PAA conjugate was not enhanced at pH 2 or 10.

3.4.2. Cationic PAM enhances the activity and stability of DAAO identified by md simulation

After demonstrating that the anionic PAA can boost the activity of Cyt C, we further investigated if cationic PAM enhances the catalytic performances of DAAO. The electrostatic surface potentials of DAAO magnified significantly with the increase of PAM grafting density (Fig. S2d) in good agreement with the zeta potential result. The electrostatic map of DAAO showed the distribution of charged patches on the surface of DAAO (Fig. 4a). Similarly, the introduction of PAM enhanced the hydrophilicity of DAAO as suggested from its larger SASA values (Fig. S12a). The number of hydrogen bonds between DAAO and
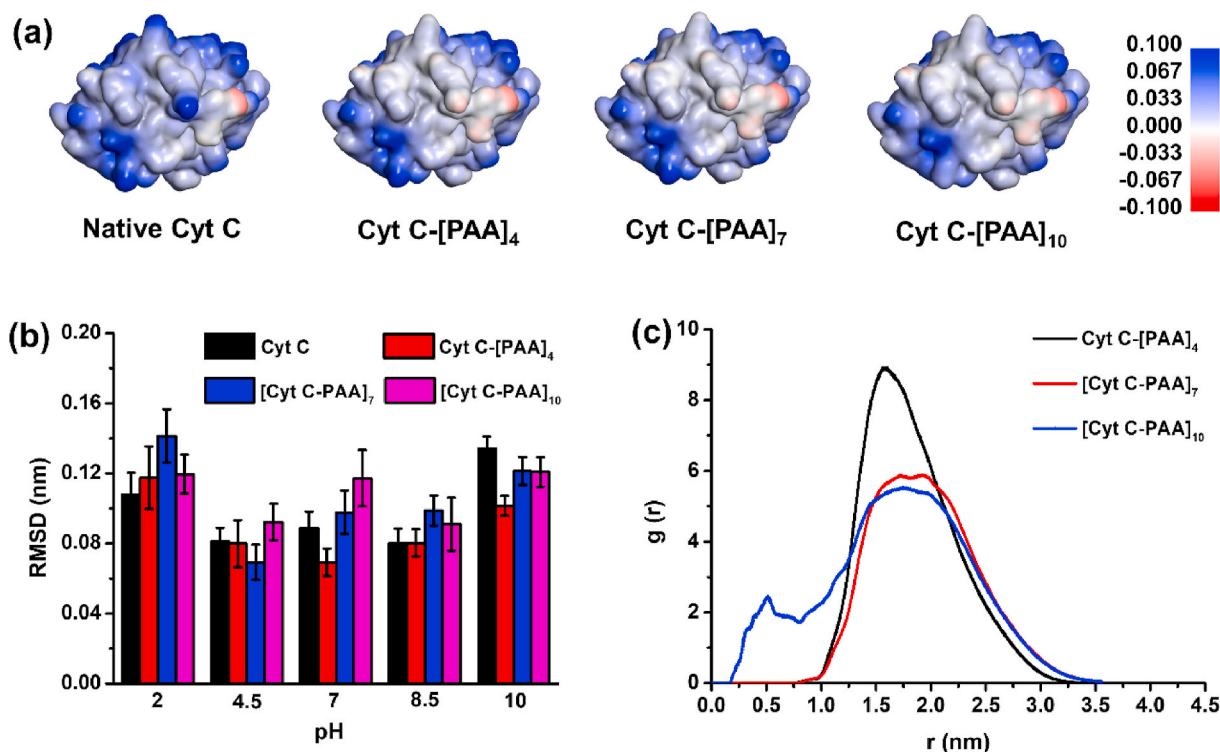
Fig. 3. The electrostatic potential map of Cyt C before and after chemical grafting with PAA (a), root-mean-square deviation (RMSD) of native Cyt C and Cyt C-[PAA]$_n$ (n = 4, 7, 10) conjugate as a function of pHs (e), and radial distribution functions (RDF) between co-enzyme heme and Lys residues in native Cyt C and Cyt C-[PAA]$_n$ (n = 4, 7, 10) conjugate as a function of pHs (f).
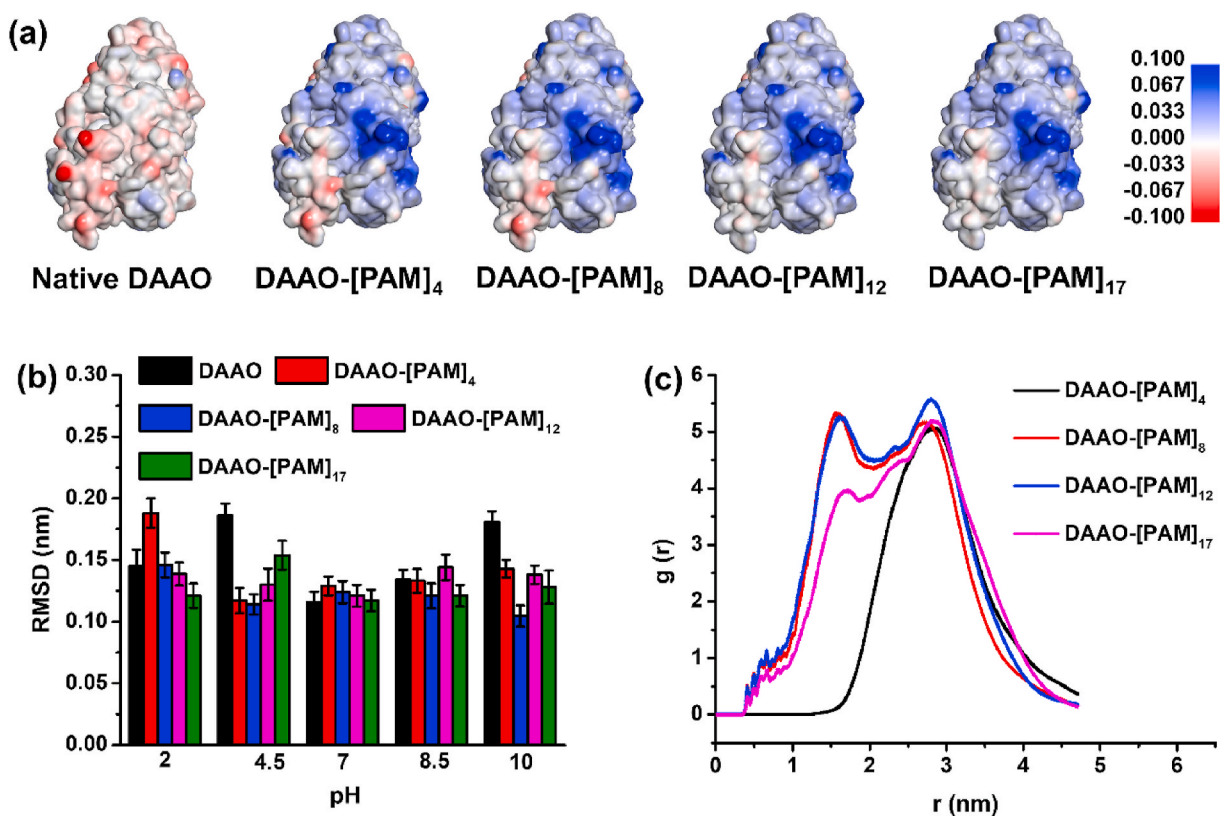
Fig. 4. The electrostatic potential map of DAAO before and after chemical grafting with PAM (a), root-mean-square deviation (RMSD) of native DAAO and DAAO-[PAM]$_n$ (n = 4, 8, 12, 17) conjugate as a function of pHs (b), and radial distribution functions (RDF) between co-enzyme FAD and Asp/Glu residues in native DAAO and DAAO-[PAM]$_n$ (n = 4, 8, 12, 17) conjugates as a function of pHs (c).

water augmented with the raise of PAM grafting density owing to the addition of amine groups (Fig. S12b). In accordance with the CD spectra in Fig. S4, the secondary structures of DAAO were not influenced after chemical modification with PAM as indicated from the simulation results (Fig. S13).

Fig. 4b exhibited a dramatically decreased RMSD value for DAAO-[PAM]$_n$ (n = 4, 8, 12, 17) conjugates than native DAAO particularly in the case of DAAO-[PAM]$_8$, indicating the possible enhancement of DAAO activity after grafting with the positively charged PAM. Radial distribution functions (RDF) between co-enzyme flavin adenine dinucleotide (FAD) and Asp/Glu residues in DAAO were given in Fig. 4c. A prominent peak starting from 4.5 nm was observed for DAAO-[PAM]$_n$ (n = 4, 8, 12, 17) conjugates, implying PAM modification occurred at Asp/Glu residues that were 4.5 nm away from FAD. The DAAO-[PAM]$_8$, DAAO-[PAM]$_{12}$, and DAAO-[PAM]$_{17}$ conjugates showed another notable peak beginning at 2.0 nm indicating part of the modified Asp and Glu residues were at a distance of 2.0 nm from FAD, and hence a larger PAM grafting density. The RMSF of 28 key amino acids in DAAO that interacted with the FAD binding sites were illustrated in Fig. S14. However, no explicit correlation can be discovered between the RMSF perturbations and enzyme activity, presumably due to the relatively large fluctuation of FAD (Fig. S15).

3.5. Exploration of protection effect of polyelectrolytes

The thermal stability of polyelectrolytes modified enzymes was also studied by evaluating their residual activities in comparison to native enzymes after conditioning at different temperatures (30, 60, and 90 °C) for 3 h. The native Cyt C retained 74.8 and 45.7% of its maximum activity at temperatures of 60 and 90 °C (Fig. 5a). By contrast, 142.4 and 121.6% of its maximum activity were still preserved at 60 and 90 °C for the Cyt C-PAA conjugate. With respect to DAAO, only 40.4% of its

maximum activity was maintained at a temperature of 60 °C for native DAAO as opposed to 54% for DAAO-PAM conjugate (Fig. 5b).

The thermodynamic stability of native and immobilized enzymes was further assessed using MD simulations by conditioning the simulation systems at 298, 313, 333, and 363 K, respectively. The RMSD was employed to investigate the conformational changes of enzymes. Decreased RMSD values were observed for Cyt C-[PAA]$_4$ and DAAO-[PAM]$_8$ conjugates in contrast with their native counterparts [Fig. 5c, d], indicating that the chemical modification of enzymes using anionic and cationic polyelectrolytes better maintained the native conformational structure of enzymes and thus showed higher thermal stability.

4. Conclusions

We have successfully matched the operational pH range for an enzyme cascade in which two enzymes have opposite pH-activity profiles by engineering the enzyme microenvironment using ionic polymers. The grafting of Cyt C with negatively charged polymer chains displays a 205.6% improvement of its maximum activity and extends the optimum pH from 4.5 to 3~7, while the conjugation of DAAO with positively charged polymer chains exhibits 128.2% improvement and the optimal pH was from 8.5 to 2~10. The catalytic efficiency of the cascade reaction is enhanced by 1.37-fold. More importantly, an in-depth mechanism study at a molecular level carried out by UV–vis/CD spectroscopy and MD simulations revealed that engineering of the local pH microenvironment of enzymes may alter the protein surface charge and aggregation state, facilitate an optimal range of interaction strengths, and thus promotes enzyme activity/stability and enhance synergistic biocatalysis of cascade reactions. This suggests that enzyme microenvironment modulation can serve as a platform for preserving the conformational structures of proteins.
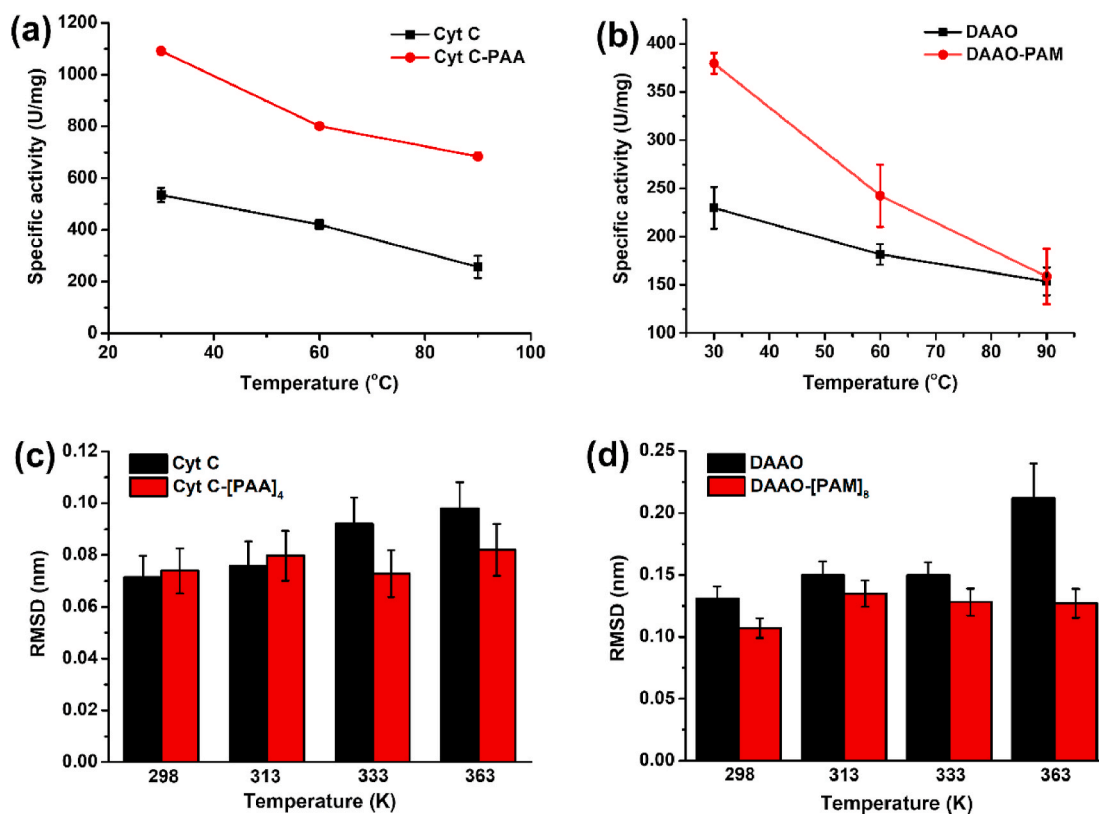
Fig. 5. Operational stabilities of native Cyt C and Cyt C-PAA conjugate (a), and native DAAO and DAAO-PAM conjugate (b) at different temperatures (30, 65, and 95 °C). Root-mean-square deviation (RMSD) of native Cyt C and Cyt C-[PAA]$_4$ conjugate (c), and native DAAO and DAAO-[PAM]$_8$ conjugate (d) at different temperatures (298, 313, 333, and 363 K).

CRediT authorship contribution statement

Jing Wang: modified enzymes and performed the enzymatic catalysis; carried out the molecular dynamic simulations. **Haiyang Zhang:** carried out the molecular dynamic simulations. **Deping Yin:** modified enzymes and performed the enzymatic catalysis. **Xiao Xu:** carried out the molecular dynamic simulations. **Tianwei Tan:** directed the projects. **Yongqin Lv:** conceived and designed the experiments, wrote the manuscript, and all authors contributed to revising the paper.

Declaration of competing interest

The authors declare no competing financial interest.

Acknowledgment

Appendix A. Supplementary data

Supplementary data to this article can be found online at https://doi.org/10.1016/j.synbio.2021.06.004.

Abbreviations

Cyt C   cytochrome C
DAAO $_D$-amino acid oxidase
PAA   poly (acrylic acid)
PAM   polyallylamine
CD   circular dichroism
HRP   horseradish peroxidase
ABTS   2,2′-azino-bis(3-ethylbenzothiazoline-6-sulphonic acid)
EDC N-(3-dimethylaminopropyl)-N'-ethylcarbodiimide hydrochloride
NHS N-hydroxysulfosuccinimide
RESP   restrained electrostatic potential
RMSD   root-mean-square deviations
RMSF   root-mean-square fluctuation
RDF   radial distribution function
SA   solvent accessibility
SASA   solvent-accessible surface area
MD   molecular dynamics
FAD   flavin adenine dinucleotide.

References

[1] Nielsen J. Yeast cell factories on the horizon. Science 2015;349:1050–1.
[2] Ro DK, Paradise EM, Ouellet M, Fisher KJ, Newman KL, Ndungu JM, Ho KA, Eachus RA, Ham TS, Kirby J, Chang MCY, Withers ST, Shiba Y, Sarpong R, Keasling JD. Production of the antimalarial drug precursor artemisinic acid in engineered yeast. Nature 2006;440:940–3.
[3] Schmid A, Dordick JS, Hauer B, Kiener A, Wubbolts M, Witholt B. Industrial biocatalysis today and tomorrow. Nature 2001;409:258–68.
[4] Jemli S, Ayadi-Zouari D, Hlima HB, Bejar S. Biocatalysts: application and engineering for industrial purposes. Crit Rev Biotechnol 2016;36:246–58.
[5] Saxena A, Singh Chauhan P. Role of various enzymes for deinking paper: a review. Crit Rev Biotechnol 2017;37:598–612.
[6] Martin VJJ, Pitera DJ, Withers ST, Newman JD, Keasling JD. Engineering a mevalonate pathway in Escherichia coli for production of terpenoids. Nat Biotechnol 2003;21:796–802.
[7] Cao X, Yang S, Cao C, Zhou YJ. Harnessing sub-organelle metabolism for biosynthesis of isoprenoids in yeast. Synth. Syst. Biotechnol. 2020;5:179–86.
[8] Chen K, Arnold FH. Engineering new catalytic activities in enzymes. Nat. Catal. 2020;3:203–13.
[9] Yang KK, Wu Z, Arnold FH. Machine-learning-guided directed evolution for protein engineering. Nat Methods 2019;16:687–94.
[10] Kan SBJ, Lewis RD, Chen K, Arnold FH. Directed evolution of cytochrome c for carbon-silicon bond formation: bringing silicon to life. Science 2016;354:1048–51.
[11] Shapiro MG, Westmeyer GG, Romero PA, Szablowski JO, Kuster B, Shah A, Otey CR, Langer R, Arnold FH, Jasanoff A. Directed evolution of a magnetic resonance imaging contrast agent for noninvasive imaging of dopamine. Nat Biotechnol 2010;28:264–70.
[12] Sun S, You C. Disaccharide phosphorylases: structure, catalytic mechanisms and directed evolution. Synth. Syst. Biotechnol. 2021;6:23–31.
[13] Liu X, Zhu X, Wang H, Liu T, Cheng J, Jiang H. Discovery and modification of cytochrome P450 for plant natural products biosynthesis. Synth. Syst. Biotechnol. 2020;5:187–99.
[14] Drufva EE, Hix EG, Bailey CB. Site directed mutagenesis as a precision tool to enable synthetic biology with engineered modular polyketide synthases. Synth. Syst. Biotechnol. 2020;5:62–80.
[15] Bornscheuer UT. Immobilizing enzymes: how to create more Suitable Biocatalysts. Angew Chem Int Ed 2003;42:3336–7.
[16] Cheng K, Svec F, Lv Y, Tan T. Hierarchical micro- and mesoporous Zn-based metal–organic frameworks templated by hydrogels: their use for enzyme immobilization and catalysis of knoevenagel reaction. Small 2019;15:1902927.
[17] Zhang Y, Ge J, Liu Z. Enhanced activity of immobilized or chemically modified enzymes. ACS Catal 2015;5:4503–13.
[18] Li Y, Wen LY, Tan TW, Lv YQ. Sequential Co-immobilization of enzymes in metal-organic frameworks for efficient biocatalytic conversion of adsorbed CO2 to formate. Front. Bioeng. Biotech. 2019;7:394.
[19] Cao Y, Wen LY, Svec F, Tan TW, Lv YQ. Magnetic AuNP@Fe3O4 nanoparticles as reusable carriers for reversible enzyme immobilization. Chem Eng J 2016;286: 272–81.
[20] Lv YQ, Lin ZX, Tan TW, Svec F. Reusable bioreactors using reversible immobilization of enzyme on monolithic porous polymer support with attached gold nanoparticles. Biotechnol Bioeng 2014;111:50–8.
[21] Naowarojna N, Cheng R, Lopez J, Wong C, Qiao L, Liu P. Chemical modifications of proteins and their applications in metalloenzyme studies. Synth. Syst. Biotechnol. 2021;6:32–49.
[22] Wu X, Xiong J, Liu S, Zong M-H, Lou W-Y. A versatile competitive coordination strategy for tailoring bioactive zeolitic imidazolate framework composites. Small 2021:2007586.
[23] Huang Z-X, Cao S-L, Xu P, Wu H, Zong M-H, Lou W-Y. Preparation of a novel nanobiocatalyst by immobilizing penicillin acylase onto magnetic nanocrystalline cellulose and its use for efficient synthesis of cefaclor. Chem Eng J 2018;346: 361–8.
[24] Liang S, Wu X-L, Xiong J, Zong M-H, Lou W-Y. Metal-organic frameworks as novel matrices for efficient enzyme immobilization: an update review. Coord Chem Rev 2020;406:213149.
[25] Wu Z, Liu C, Zhang Z, Zheng R, Zheng Y. Amidase as a versatile tool in amide-bond cleavage: from molecular features to biotechnological applications. Biotechnol Adv 2020;43:107574.
[26] Lin C, Xu K, Zheng R, Zheng Y. Immobilization of amidase into a magnetic hierarchically porous metal–organic framework for efficient biocatalysis. Chem Commun 2019;55(40):5697–700.
[27] Garcia-Galan C, Berenguer-Murcia Á, Fernandez-Lafuente R, Rodrigues RC. Potential of different enzyme immobilization strategies to improve enzyme performance. Adv Synth Catal 2011;353:2885–904.
[28] Ge J, Lei J, Zare RN. Protein–inorganic hybrid nanoflowers. Nat Nanotechnol 2012; 7:428–32.
[29] Chen W-H, Vázquez-González M, Zoabi A, Abu-Reziq R, Willner I. Biocatalytic cascades driven by enzymes encapsulated in metal–organic framework nanoparticles. Nat. Catal. 2018;1:689–95.
[30] Li Y, Wen L, Qu Y, Lv Y. Metal–enzyme hybrid microspheres assembled via Mg^{2+}-allosteric effector. Ind Eng Chem Res 2020;59:20278–84.
[31] An HD, Song J, Wang T, Xiao NN, Zhang ZJ, Cheng P, Ma SQ, Huang H, Chen Y. Metal-Organic framework disintegrants: enzyme preparation platforms with boosted activity. Angew Chem Int Ed 2020;59:16764–9.
[32] Lyu F, Zhang Y, Zare RN, Ge J, Liu Z. One-pot synthesis of protein-embedded metal-organic frameworks with enhanced biological activities. Nano Lett 2014;14: 5761–5.
[33] Brogan APS, Bui-Le L, Hallett JP. Non-aqueous homogenous biocatalytic conversion of polysaccharides in ionic liquids using chemically modified glucosidase. Nat Chem 2018;10:859–65.
[34] Lancaster L, Abdallah W, Banta S, Wheeldon I. Engineering enzyme microenvironments for enhanced biocatalysis. Chem Soc Rev 2018;47:5177–86.
[35] Wang L, Li X, Yuan L, Wang H, Chen H, Brash JL. Improving the protein activity and stability under acidic conditions via site-specific conjugation of a pH-responsive polyelectrolyte. J Math Chem B 2015;3:498–504.
[36] J. Thiele, M., Davari MD, König M, Hofmann I, Junker NO, Mirzaei Garakani T, Vojcic L, Fitter J, Schwaneberg U. Enzyme–polyelectrolyte complexes boost the catalytic performance of enzymes. ACS Catal 2018;8(11):10876–87.
[37] Shutava TG, Kommireddy DS, Lvov YM. Layer-by-Layer enzyme/polyelectrolyte films as a functional protective barrier in oxidizing media. J Am Chem Soc 2006; 128:9926–34.
[38] Levin Y, Pecht M, Goldstein L, Katchalski E. A water-insoluble polyanionic derivative of trypsin. I. Preparation and properties. Biochemistry 1964;3:1905–13.
[39] Goldstein L, Levin Y, Katchalski E. A water-insoluble polyanionic derivative of trypsin. II. Effect of the polyelectrolyte carrier on the kinetic behavior of the bound trypsin. Biochemistry 1964;3:1913–9.

[40] Goldstein L, Pecht M, Blumberg S, Atlas D, Levin Y. Water-insoluble enzymes. Synthesis of a new carrier and its utilization for preparation of insoluble derivatives of papain, trypsin, and subtilopeptidase A. Biochemistry 1970;9:2322–34.

[41] Yan M, Ge J, Dong W, Liu Z, Ouyang P. Preparation and characterization of a temperature-sensitive sulfobetaine polymer-trypsin conjugate. Biochem Eng J 2006;30:48–54.

[42] Zhang Y, Wang Q, Hess H. Increasing enzyme cascade throughput by pH-engineering the microenvironment of individual enzymes. ACS Catal 2017;7: 2047–51.

[43] Fu J, Yang YR, Johnson-Buck A, Liu M, Liu Y, Walter NG, Woodbury NW, Yan H. Multi-enzyme complexes on DNA scaffolds capable of substrate channelling with an artificial swinging arm. Nat Nanotechnol 2014;9:531–6.

[44] Murata H, Cummings CS, Koepsel RR, Russell AJ. Rational tailoring of substrate and inhibitor affinity via ATRP polymer-based protein engineering. Biomacromolecules 2014;15:2817–23.

[45] Zhang Y, Tsitkov S, Hess H. Proximity does not contribute to activity enhancement in the glucose oxidase-horseradish peroxidase cascade. Nat Commun 2016:13982.

[46] Kurinomaru T, Tomita S, Hagihara Y, Shiraki K. Enzyme hyperactivation system based on a complementary charged pair of polyelectrolytes and substrates. Langmuir 2014;30:3826–31.

[47] Lee EH, Tsujimoto T, Uyama H, Sung MH, Kim K, Kuramitsu S. Enhancement of enzyme activity and stability by poly(gamma-glutamic acid). Polym J 2010;42: 818–22.

[48] Dos Santos JP, Zavareze EdR, Dias ARG, Vanier NL. Immobilization of xylanase and xylanase–β-cyclodextrin complex in polyvinyl alcohol via electrospinning improves enzyme activity at a wide pH and temperature range. Int J Biol Macromol 2018; 118:1676–84.

[49] Sun Y, Li Z, Wu J, Wang Z, Dong Y, Wang H, Brash JL, Yuan L, Chen H. Gold nanoparticle–protein conjugate dually-responsive to pH and temperature for modulation of enzyme activity. J Math Chem B 2019;7:3260–7.

[50] Liang J, Gao S, Liu J, Zulkifli MY, Xu J, Scott J, Chen V, Shi J, Rawal A, Liang K. Hierarchically porous biocatalytic MOF microreactor as a versatile platform towards enhanced multienzyme and cofactor-dependent biocatalysis. Angew Chem Int Ed 2021;133:2–10.

[51] Sperl JM, Sieber V. Multienzyme cascade reactions-status and recent advances. ACS Catal 2018;8:2385–96.

[52] Gao S, Wang Z, Ma L, Liu Y, Gao J, Jiang Y. Mesoporous core–shell nanostructures bridging metal and biocatalyst for highly efficient cascade reactions. ACS Catal 2020;10:1375–80.

[53] Che SY, Wang J, Ji XY, Su ZG, Wang SM, Zhang SP. Positional assembly of multi-enzyme cascade reaction in polyelectrolyte doped microcapsule through electrospray and layer-by-layer assembly. Synth. Syst. Biotechnol. 2020;5:206–13.

[54] Ji XJ, Su ZG, Wang P, Ma GH, Zhang SP. Tethering of nicotinamide adenine dinucleotide inside hollow nanofibers for high-yield synthesis of methanol from carbon dioxide catalyzed by coencapsulated multienzymes. ACS Nano 2015;9: 4600–10.

[55] Gordon JC, Myers JB, Folta T, Shoja V, Heath LS, Onufriev A. H++: a server for estimating pK_as and adding missing hydrogens to macromolecules. Nucleic Acids Res 2005;33:W368–71.

[56] Maier JA, Martinez C, Kasavajhala K, Wickstrom L, Hauser KE, Simmerling C. ff14SB: improving the accuracy of protein side chain and backbone parameters from ff99SB. J Chem Theor Comput 2015;11:3696–713.

[57] Frisch MJTGW, Schlegel HB, Scuseria GE, Robb MA, Cheeseman JR, Scalmani G, Barone V, Mennucci B, Petersson GA, Nakatsuji H, Caricato M, Li X, Hratchian HP, Izmaylov AF, Bloino J, Zheng G, Sonnenberg JL, Hada M, Ehara M, Toyota K, Fukuda R, Hasegawa J, Ishida M, Nakajima T, Honda Y, Kitao O, Nakai H, Vreven T, Montgomery JA, Peralta JE, Ogliaro F, Bearpark M, Heyd JJ, Brothers E, Kudin KN, Staroverov VN, Kobayashi R, Normand J, Raghavachari K, Rendell A, Burant JC, Iyengar SS, Tomasi J, Cossi M, Rega N, Millam JM, Klene M, Knox JE, Cross JB, Bakken V, Adamo C, Jaramillo J, Gomperts R, Stratmann RE, Yazyev O, Austin AJ, Cammi R, Pomelli C, Ochterski JW, Martin RL, Morokuma K, Zakrzewski VG, Voth GA, Salvador P, Dannenberg JJ, Dapprich S, Daniels AD, Farkas, Foresman JB, Ortiz JV, Cioslowski J, Fox D. Gaussian 09, revision B.01. Wallingford, CT: Gaussian, Inc.; 2009.

[58] Wang J, Wang W, Kollman PA, Case DA. Automatic atom type and bond type perception in molecular mechanical calculations. J Mol Graph Model 2006;25: 247–60.

[59] Ahmad S, Gromiha M, Fawareh H, Sarai A. ASAView: database and tool for solvent accessibility representation in proteins. BMC Bioinf 2004;5:51.

[60] Abraham MJ, Murtola T, Schulz R, Páll S, Smith JC, Hess B, Lindahl E. GROMACS: high performance molecular simulations through multi-level parallelism from laptops to supercomputers. Software 2015;1–2:19–25.

[61] Parrinello M, Rahman A. Polymorphic transitions in single crystals: a new molecular dynamics method. J Appl Phys 1981;52:7182–90.

[62] Nosé S, Klein ML. Constant pressure molecular dynamics for molecular systems. Mol Phys 1983;50:1055–76.

[63] Essmann U, Perera L, Berkowitz ML, Darden T, Lee H, Pedersen LG. A smooth particle mesh Ewald method. J Chem Phys 1995;103:8577–93.

[64] Darden T, York D, Pedersen L. Particle mesh Ewald: an N·log(N) method for Ewald sums in large systems. J Chem Phys 1993;98:10089–92.

[65] Humphrey W, Dalke A, Schulten K. VMD: visual molecular dynamics. J Mol Graph Model 1996;14:33–8.

[66] Liu Q, Chen L, Zhang Z, Du B, Xiao Y, Yang K, Gong L, Wu L, Li X, He Y. PH-dependent enantioselectivity of D-amino acid oxidase in aqueous solution. Sci Rep 2017;7:2994.

[67] Bihari M, Russell TP, Hoagland DA. Dissolution and dissolved state of cytochrome c in a neat, hydrophilic ionic liquid. Biomacromolecules 2010;11:2944–8.

[68] Sahoo DK, Jena S, Tulsiyan KD, Dutta J, Chakrabarty S, Biswal HS. Amino-acid-based ionic liquids for the improvement in stability and activity of cytochrome c: a combined experimental and molecular dynamics study. J Phys Chem B 2019;123: 10100–9.

[69] Singh UK, Kumari M, Khan SH, Bohidar HB, Patel R. Mechanism and dynamics of long-term stability of cytochrome c conferred by long-chain imidazolium ionic liquids at low concentration. ACS Sustain Chem Eng 2018;6:803–15.

[70] Tajima H, Ikeda S, Matsuda M, Hanasaki N, Oh J-W, Akiyama H. A light-emitting diode fabricated from horse-heart cytochrome c. Solid State Commun 2003;126: 579–81.

[71] Liu Q, Chen L, Zhang Z, Du B, Xiao Y, Yang K, Gong L, Wu L, Li X, He Y. PH-dependent enantioselectivity of D-amino acid oxidase in aqueous solution. Sci Rep 2017;7:2994.

[72] Zaboli M, Raissi H, Zaboli M, Farzad F, Torkzadeh-Mahani M. Stabilization of D-lactate dehydrogenase diagnostic enzyme via immobilization on pristine and carboxyl-functionalized carbon nanotubes, a combined experimental and molecular dynamics simulation study. Arch Biochem Biophys 2019;661:178–86.

[73] Housaindokht MR, Bozorgmehr MR, Monhemi H. Structural behavior of *Candida antarctica* lipase B in water and supercritical carbon dioxide: a molecular dynamic simulation study. J Supercrit Fluids 2012;63:180–6.